Prepared for submission to JHEP

Measurement of time-dependent CP asymmetries in $B^0 \to K^0_S \pi^+\pi^-\gamma$ decays at Belle and Belle II

The Belle and Belle II Collaborations

M. Abumusabh, I. Adachi, L. Aggarwal, H. Ahmed, Y. Ahn, H. Aihara, N. Akopov, S. Alghamdi, M. Alhakami, K. Amos, N. Anh Ky, D. M. Asner, H. Atmacan, T. Aushev, R. Ayad, V. Babu, S. Bahinipati, P. Bambade, Sw. Banerjee, M. Barrett, M. Bartl, J. Baudot, A. Beaubien, F. Becherer, J. Becker, J. V. Bennett, V. Bertacchi, E. Bertholet, M. Bessner, S. Bettarini, V. Bhardwaj, B. Bhuyan, F. Bianchi, T. Bilka, D. Biswas, A. Bobrov, D. Bodrov, J. Borah, A. Boschetti, A. Bozek, M. Bračko, P. Branchini, R. A. Briere, T. E. Browder, A. Budano, S. Bussino, Q. Campagna, M. Campajola, G. Casarosa, C. Cecchi, P. Cheema, C. Chen, L. Chen, C. Cheshta, H. Chetri, J. Chin, K. Chirapatpimol, H.-E. Cho, K. Cho, S.-J. Cho, S.-K. Choi, S. Choudhury, J. A. Colorado-Caicedo, L. Corona, J. X. Cui, E. De La Cruz-Burelo, S. A. De La Motte, G. De Nardo, G. De Pietro, R. de Sangro, M. Destefanis, A. Di Canto, Z. Doležal, I. Domínguez Jiménez, T. V. Dong, X. Dong, M. Dorigo, G. Dujany, P. Ecker, J. Eppelt, R. Farkas, P. Feichtinger, T. Ferber, T. Fillinger, C. Finck, G. Finocchiaro, F. Forti, B. G. Fulsom, A. Gale, M. Garcia-Hernandez, R. Garg, G. Gaudino, V. Gaur, V. Gautam, A. Gaz, A. Gellrich, G. Ghevondyan, D. Ghosh, H. Ghumaryan, G. Giakoustidis, R. Giordano, A. Giri, P. Gironella Gironell, R. Godang, O. Gogota, P. Goldenzweig, W. Gradl, E. Graziani, D. Greenwald, Y. Guan, K. Gudkova, I. Haide, Y. Han, H. Hayashii, S. Hazra, M. T. Hedges, A. Heidelbach, G. Heine, I. Heredia de la Cruz, M. Hernández Villanueva, T. Higuchi, M. Hohmann, R. Hoppe, P. Horak, X. T. Hou, C.-L. Hsu, T. Humair, T. Iijima, N. Ipsita, A. Ishikawa, R. Itoh, M. Iwasaki, P. Jackson, W. W. Jacobs, E.-J. Jang, S. Jia, Y. Jin, A. Johnson, K. H. Kang, F. Keil, C. Ketter, C. Kiesling, D. Y. Kim, J.-Y. Kim, K.-H. Kim, H. Kindo, K. Kinoshita, P. Kodyš, T. Koga, S. Kohani, K. Kojima, A. Korobov, S. Korpar, E. Kovalenko, R. Kowalewski, P. Križan, P. Krokovny, T. Kuhr, Y. Kulii, D. Kumar, R. Kumar, K. Kumara, T. Kunigo, Y.-J. Kwon, S. Lacaprara, T. Lam, T. S. Lau,

M. Laurenza, F. R. Le Diberder, H. Lee, M. J. Lee, P. Leo, C. Li, H.-J. Li, L. K. Li, Q. M. Li, W. Z. Li, Y. Li, Y. B. Li, Y. P. Liao, J. Libby, J. Lin, S. Lin, Z. Liptak, M. H. Liu, Q. Y. Liu, Z. Liu, D. Liventsev, S. Longo, T. Lueck, C. Lyu, J. L. Ma, Y. Ma, M. Maggiora, R. Maiti, G. Mancinelli, R. Manfredi, E. Manoni, M. Mantovano, D. Marcantonio, C. Marinas, C. Martellini, A. Martens, T. Martinov, L. Massaccesi, M. Masuda, S. K. Maurya, M. Maushart, J. A. McKenna, Z. Mediankin Gruberová, F. Meier, D. Meleshko, M. Merola, C. Miller, M. Mirra, K. Miyabayashi, H. Miyake, S. Moneta, A. L. Moreira de Carvalho, H.-G. Moser, H. Murakami, R. Mussa, I. Nakamura, M. Nakao, Z. Natkaniec, A. Natochii, M. Nayak, M. Neu, S. Nishida, R. Nomaru, S. Ogawa, R. Okubo, H. Ono, G. Pakhlova, A. Panta, S. Pardi, J. Park, S.-H. Park, A. Passeri, S. Patra, S. Paul, T. K. Pedlar, R. Pestotnik, M. Piccolo, L. E. Piilonen, T. Podobnik, C. Praz, S. Prell, E. Prencipe, M. T. Prim, H. Purwar, P. Rados, S. Raiz, K. Ravindran, J. U. Rehman, M. Reif, S. Reiter, L. Reuter, D. Ricalde Herrmann, I. Ripp-Baudot, G. Rizzo, S. H. Robertson, J. M. Roney, A. Rostomyan, N. Rout, S. Saha, L. Salutari, D. A. Sanders, S. Sandilya, L. Santelj, B. Scavino, G. Schnell, M. Schnepf, K. Schoenning, C. Schwanda, Y. Seino, K. Senyo, C. Sfienti, W. Shan, X. D. Shi, T. Shillington, T. Shimasaki, J.-G. Shiu, D. Shtol, A. Sibidanov, F. Simon, J. Skorupa, R. J. Sobie, M. Sobotzik, A. Soffer, E. Solovieva, S. Spataro, B. Spruck, M. Starič, P. Stavroulakis, S. Stefkova, R. Stroili, M. Sumihama, K. Sumisawa, H. Svidras, M. Takahashi, M. Takizawa, U. Tamponi, S. S. Tang, K. Tanida, F. Tenchini, T. Tien Manh, O. Tittel, R. Tiwary, E. Torassa, K. Trabelsi, F. F. Trantou, I. Tsaklidis, I. Ueda, K. Unger, Y. Unno, K. Uno, S. Uno, P. Urquijo, S. E. Vahsen, R. van Tonder, K. E. Varvell, M. Veronesi, V. S. Vismaya, L. Vitale, V. Vobbilisetti, R. Volpe, M. Wakai, S. Wallner, M.-Z. Wang, A. Warburton, S. Watanuki, C. Wessel, X. P. Xu, B. D. Yabsley, W. Yan, J. Yelton, K. Yi, J. H. Yin, K. Yoshihara, C. Z. Yuan, J. Yuan, L. Zani, M. Zeyrek, B. Zhang, V. Zhilich, J. S. Zhou, Q. D. Zhou, L. Zhu, R. Žlebčík

Abstract: We present a measurement of the time-dependent *CP* asymmetry in $B^0 \to K^0_S\,\pi^+\pi^-\gamma$ decays using a data set of 365 fb^{-1} recorded by the Belle II experiment and the final data set of 711 fb^{-1} recorded by the Belle experiment at the $\Upsilon(4S)$ resonance. The direct and mixing-induced time-dependent *CP* violation parameters C and S are determined along with two additional quantities, S^+ and S^-, defined in the two halves of the $m^2(K^0_S\pi^+) - m^2(K^0_S\pi^-)$ plane. The measured values are $C = -0.17 \pm 0.09 \pm 0.04$, $S = -0.29 \pm 0.11 \pm 0.05$, $S^+ = -0.57 \pm 0.23 \pm 0.10$ and $S^- = 0.31 \pm 0.24 \pm 0.05$, where the first uncertainty is statistical and the second systematic.

Contents

1 Introduction

Flavor-changing neutral currents, in particular $b \to s\gamma$ transitions, are sensitive probes of the Standard Model (SM) of particle physics [1–3]. The emitted photon in these transitions is predominantly left-handed. A right-handed photon is predicted to occur only due to a chirality flip of the outgoing s-quark line, which is suppressed by a factor proportional to m_s^2/m_b^2. Therefore, in decays of $\overline{B}^0$ and B^0 mesons to a CP eigenstate and a photon, denoted as $B^0 \to f_{CP}\gamma$, the mixing-induced CP violation is predicted to be very small. Physics beyond the SM may enhance the mixing-induced CP violation by increasing the right-handed current contribution to these transitions. Measurement of the mixing-induced CP asymmetry in these decay channels probes those non-SM processes that result in larger CP asymmetries.

At the KEKB and SuperKEKB colliders, pairs of B mesons in a coherent quantum state are produced through e^+e^- collisions at the $\Upsilon(4S)$ resonance. The B mesons are referred to as B_{sig} and B_{tag}, where B_{sig} is the meson of interest and B_{tag} is the meson whose information is used to infer the flavor (B^0 or $\overline{B}^0$) of B_{sig} at the time the B_{tag} decays. The time-dependent CP asymmetry in neutral B mesons decaying to a final state $f_{CP}\gamma$ is defined as

$$\mathcal{A}_{CP}(\Delta t) = \frac{\Gamma(B_{\text{tag}=B^0}(\Delta t) \to f_{CP}\gamma) - \Gamma(B_{\text{tag}=\overline{B}^0}(\Delta t) \to f_{CP}\gamma)}{\Gamma(B_{\text{tag}=B^0}(\Delta t) \to f_{CP}\gamma) + \Gamma(B_{\text{tag}=\overline{B}^0}(\Delta t) \to f_{CP}\gamma)}$$

where $\Gamma(B_{\text{tag}=B^0}(\Delta t))$ is the decay rate of a B meson for which its companion has been tagged as a B^0 at decay, and $\Delta t \equiv t_{\text{sig}} - t_{\text{tag}}$ corresponds to the difference between the proper decay times of the $B_{\rm sig}$ and $B_{\rm tag}$. It can be parameterized as follows:

$$\mathcal{A}_{CP}(\Delta t) = S\sin(\Delta m \Delta t) - C\cos(\Delta m \Delta t), \tag{1.1}$$

where S and C are known as the mixing-induced and direct CP violation parameters, respectively, and Δm is the mass difference between the heavy and light mass eigenstates of the neutral B mesons. The BaBar and Belle experiments have reported measurements [4, 5] of the time-dependent CP asymmetries for the $B^0 \to K_S^0\pi^+\pi^-\gamma$ decay, with uncertainties at the level of 25% (the Belle measurement was performed on a subset of the full Belle data).

This paper presents the combined measurement of the time-dependent CP asymmetry in $B^0 \to K_S^0\pi^+\pi^-\gamma$ decays using the entire Belle dataset, 711 fb^{-1}, and 365 fb^{-1} of data recorded between 2019 and 2022 by Belle II.

The channel of interest is the $B^0 \to K_{\rm res}\gamma \to (K_S^0\pi^+\pi^-)\gamma$ decay, where the intermediate resonance $K_{\rm res}$ decays into a K_S^0 and a charged-pion pair. Among the many possible intermediate resonances only those that decay through the two-body $K_{\rm res} \to K_S^0\rho^0$ channel are true CP eigenstates. For this measurement, we only consider the decay of K_S^0 to two charged pions, $K_S^0 \to \pi^+\pi^-$, while the ρ^0 meson is reconstructed using its main decay mode, $\rho^0 \to \pi^+\pi^-$. The time-dependent CP asymmetry we measure has, in addition to the CP eigenstate $B^0 \to K_S^0\rho^0\gamma$ mode, contributions from non-CP eigenstates involving strange meson resonances. The most important of these are

$$B^0 \to K_{\rm res}\gamma \to (K^{*\pm}\pi^{\mp})\gamma \to ((K_S^0\pi^{\pm})\pi^{\mp})\gamma \tag{1.2}$$
$$B^0 \to K_{\rm res}\gamma \to ((K\pi)_0^{\pm}\pi^{\mp})\gamma \to ((K_S^0\pi^{\pm})\pi^{\mp})\gamma, \tag{1.3}$$

where $(K\pi)_0^{\pm}$ represents a $K\pi$ pair in an S-wave configuration. The contributions of these modes to the effective time-dependent CP asymmetries could be determined through a full amplitude analysis [4–6] of the isospin partner mode $B^+ \to K^+\pi^+\pi^-\gamma$, which would provide a full description of the amplitudes and interferences present in the $K_{\rm res}$ system. No amplitude analysis is performed in this work, but the isospin partner channel is used to validate aspects of the analysis strategy.

In addition to the measurement of the time-dependent CP asymmetries, S and C, we measure two new CP observables, proposed in Ref. [6]. We construct these new CP observables from a combined measurement of the time-dependent CP asymmetry in two halves of the $(m^2(K_S^0\pi^+), m^2(K_S^0\pi^-))$ plane defined by the inequalities $m^2(K_S^0\pi^+) \lessgtr m^2(K_S^0\pi^-)$. To ease the notation, in subsequent sections we refer to the half-plane where $m^2(K_S^0\pi^+) > m^2(K_S^0\pi^-)$ as the "up" half while the opposite half is referred to as the "down" half. Following this notation, the two new observables are defined as

$$S^+ = S^{\rm up} + S^{\rm down}$$
$$S^- = S^{\rm up} - S^{\rm down},$$

where $S^{\rm up}$ and $S^{\rm down}$ are the values of S, defined in Eq. 1.1, measured in the two half-planes. These new CP observables can be combined with two parameters (a, b), that can be extracted from an amplitude analysis of the isospin partner channel. These parameters describe the different proportions and the interference properties of the *CP* mode with respect to the non-*CP*-eigenstate modes. These four quantities, taken together, could provide constraints on the photon polarization in the $B^0 \to K_{\rm res}\gamma \to (K_S^0\pi^+\pi^-)\gamma$ mode.

The candidate selection and fit strategy are developed and validated before accessing the data containing the signal mode. Throughout this paper, the inclusion of the charge conjugate decay mode is implied unless otherwise specified.

The outline of this paper is as follows: we present the detectors, Belle and Belle II, and the corresponding data samples in Sec. 2 and Sec. 3, respectively. The reconstruction and selection of candidates from the decay channel of interest, $B^0 \to K_S^0\pi^+\pi^-\gamma$, and of its isospin partner are described in Sec. 4. We discuss the strategy to extract the *CP* observables and the associated uncertainties in Sec. 5. Finally, we present the results of the measurement and our conclusions in Sec. 6.

2 The Belle and Belle II experiments

The Belle and Belle II detectors both have a cylindrical geometry whose symmetry axis z is nearly aligned with the electron beam direction at the interaction point. The polar angle θ is defined relative to the z axis.

The Belle detector [7, 8] was located at the KEKB e^+e^- accelerator [9], which collided electrons and positrons at and near the $\Upsilon(4S)$ resonance with beam energies of 8 GeV and 3.5 GeV, respectively. It recorded data from 1999 to 2010. The Belle detector was a large-solid-angle magnetic spectrometer composed of a silicon vertex detector (SVD), where two different configurations of the silicon vertex detector and beam pipe radius were used over the course of the experiment, a central drift chamber (CDC), an array of aerogel threshold Cherenkov counters (ACC), a barrel-shaped arrangement of time-of-flight (TOF) scintillation counters, and an electromagnetic calorimeter (ECL) comprised of CsI(Tl) crystals located inside a superconducting solenoid coil that provided a magnetic field of 1.5 T. An iron flux-return yoke, placed outside the coil, was instrumented with resistive-plate chambers to detect K_L^0 mesons and identify muons. The SVD and CDC were used to reconstruct charged particle tracks and vertices, the ACC and TOF, along with ionization energy-loss (dE/dx) measurements from the CDC, were used for charged particle identification (PID) purposes, and photons were reconstructed from clusters in the ECL.

The Belle II detector [10] is located at the SuperKEKB accelerator, which collides electrons and positrons at and near the $\Upsilon(4S)$ resonance [11] with beam energies of 7 GeV and 4 GeV, respectively. The Belle II detector [10] has a cylindrical geometry and includes a two-layer silicon-pixel detector (PXD) surrounded by a four-layer double-sided SVD [12] and a 56-layer CDC. These detectors reconstruct tracks from charged particles. Only one sixth of the second layer of the PXD was installed for the data analysed here. Surrounding the CDC, which also provides dE/dx energy-loss measurements, there is a time-of-propagation counter (TOP) [13] in the central region and an aerogel-based ring-imaging Cherenkov counter (ARICH) in the forward region. These detectors provide charged-particle identification. Surrounding the TOP and ARICH there is an ECL based on CsI(Tl) crystals that primarily provides energy and timing measurements for photons and electrons. Outside of the ECL there is a superconducting solenoid magnet. Its flux return is instrumented with resistive-plate chambers and plastic scintillator modules to detect muons, K_L^0 mesons, and neutrons. The solenoid magnet provides a 1.5 T magnetic field that is oriented parallel to the z axis.

3 Datasets

This measurement is based on 365 fb^{-1} of data recorded by the Belle II experiment and 711 fb^{-1} recorded by the Belle experiment, both at the $\Upsilon(4\mathrm{S})$ resonance. Additional data samples, 43 fb^{-1} for Belle II and 86 fb^{-1} for Belle, recorded below the $\Upsilon(4\mathrm{S}) \rightarrow B\overline{B}$ threshold are used for background studies.

We use several Monte-Carlo simulated samples (MC samples) to model, study, and validate different parts of the measurement process. Samples of $e^+e^- \rightarrow \Upsilon(4\mathrm{S}) \rightarrow B\overline{B}$ are generated, together with the subsequent particle decays, using the EvtGen [14] program interfaced to the Pythia 8 (Pythia 6) software [15] for Belle II (Belle). Quark-antiquark pairs created in the $e^+e^- \rightarrow q\bar{q}$ process ($q = u, d, s, c$), referred to as continuum events, are generated with the KKMC [16] package together with Pythia 8 (Pythia 6) to handle the fragmentation process. The detector response is simulated by the Geant 4 (Geant 3) [17] package. The simulated samples include the effects of beam-induced background, as described in Ref. [18]. We use MC samples from generic e^+e^- collisions, i.e., combining $B^0\overline{B}^0$, B^+B^- and $q\bar{q}$ samples, and also specific samples of $B\overline{B}$, where one of the B mesons decays into a specified mode of interest (signal MC). We use generic MC samples corresponding to four (six) times the data luminosity for the Belle II (Belle) analysis. In addition, in Belle, we use a sample of specific rare $B\overline{B}$ decays with fifty times the recorded Belle luminosity to study other decay modes that may affect our measurement as background sources. The signal MC samples are substantially larger than the generic ones, and are generated with a single intermediate resonance, $K_{\mathrm{res}} = K_1(1270) \rightarrow K_S^0\rho$ for both Belle and Belle II analyses.

We use the Belle II analysis software [19, 20] to process both collision data and the simulated MC samples in Belle II, while we use a specific Belle analysis and software framework for Belle.

4 Candidate selection

The trigger system selects events based on the number of charged and neutral particles, along with the total ECL energy deposition, and retains hadronic $B\overline{B}$ events with an efficiency close to 100% for the signal decay mode.

In each event, the B_{sig} meson is reconstructed first, and the remaining reconstructed particles are assigned to the B_{tag} decay. The B_{sig} candidate selection is optimized to enhance the signal contribution relative to background contributions. While the selection criteria are largely similar between Belle and Belle II, differences emerge due to differences in detector performance and background conditions. Candidate $\Upsilon(4S)$ events are required to have a minimum of 4 (3) charged tracks for Belle II (Belle) and a visible energy of at least 4 GeV.

Candidate signal photons are reconstructed from ECL clusters with no associated track and with energies higher than 1.5 (1.4) GeV for Belle II (Belle). An upper bound is set on the energy of these ECL clusters at 4 (3.5) GeV to remove photon candidates arising from beam background. The photon polar angle must satisfy $\cos\theta_\gamma \in [-0.87, 0.95]$ ($[-0.65, 0.86]$). Multivariate classifiers that combine information from the photon candidate and the rest of the event are used to remove photon candidates from $\pi^0 \to \gamma\gamma$ and $\eta \to \gamma\gamma$ decays [21, 22].

The pion candidates that arise directly from the $K_{\rm res}$ decay, and not through the subsequent K_S^0 decay, are referred to as prompt pions. The corresponding charged tracks are required to point to the beam interaction region with a longitudinal distance smaller than 3 cm and a transverse distance smaller than 0.5 (1) cm for Belle II (Belle). Using the PID system, a loose requirement is placed on these tracks to be compatible with a pion hypothesis.

The K_S^0 candidates are formed by combining two opposite-sign charged particle tracks displaced with respect to the IP, and their invariant mass, assuming they are pions, is required to be within $\pm 20\,\text{MeV}/c^2$ of the known K_S^0 mass. The K_S^0 invariant mass resolution is about $6\,\text{MeV}/c^2$. Additionally, a multivariate classifier is used to determine the likelihood of the candidate to be a K_S^0, using the kinematic information from the tracks and their combination, the flight length of the K_S^0 candidate and the number of hits in the vertex detectors. In Belle the algorithm is based on a NeuroBayes Neural Network [23, 24], while in Belle II we use a Boosted Decision Tree (BDT) [25].

The $K_{\rm res}$ candidates are constructed by summing the four momenta of the prompt pions and K_S^0 candidates. The $K_{\rm res}$ candidates are required to have an invariant mass $m_{K_{\rm res}} \in [0.9, 1.8]\,\text{GeV}/c^2$, which allows higher mass structures arising from B decay backgrounds containing a charm meson to be removed. Their momentum in the center of mass (c.m.) frame is required to satisfy $p^*_{K_{\rm res}} \in [1, 3.5]$ GeV/c; no candidates arising from the signal mode are expected outside this range. The $B_{\rm sig}$ candidates are constructed by combining the four-momenta of the $K_{\rm res}$ and photon candidates. The reconstructed decay vertex of the $B_{\rm sig}$ candidate is indistinguishable from the decay vertex of the $K_{\rm res}$, since the latter decays via the strong force. We determine the $B_{\rm sig}$ vertex position by performing a fit, using only the prompt pion tracks, while constraining the $B_{\rm sig}$ to come from the beam interaction region. We only keep $B_{\rm sig}$ candidates for which the vertex fit has converged. The effect of adding the K_S^0 information into the reconstructed vertex is found to be negligible, so this information was not used. The momenta of all particles, including the photon, in the $B_{\rm sig}$ decay are recomputed after the vertex fit. Additionally, the $B_{\rm sig}$ are required to have $M_{\rm bc} > 5.20$ GeV/c^2 and $\Delta E \in [-0.2, 0.2]$ GeV, where the beam-energy-constrained mass and energy difference are defined as $M_{\rm bc} \equiv \sqrt{(\sqrt{s}/2)^2 - p_B^{*2}}$ and $\Delta E \equiv E^*_B - \sqrt{s}/2$. The variables p^*_B, E^*_B are the momentum and the energy of the B meson in the c.m. frame, respectively, and $\sqrt{s}$ is the c.m. energy of the e^+e^- collision. An additional requirement is imposed on the invariant mass of the two prompt pions forming the ρ^0, $m_{\pi^+\pi^-} \in [0.6, 0.9]\,\mathrm{GeV}/c^2$. This last requirement is the only selection step that enhances the f_{CP} contribution to the $B^0 \to K_{\mathrm{res}}\gamma$ mode.

The B_{tag} vertex is reconstructed by combining the tracks in the event that have not been used in the reconstruction of the B_{sig} [26]. The position of its decay vertex is determined by constraining the B_{tag} direction, computed as the difference between the position vector of the decay vertex and the position vector of the center of the interaction region, to be collinear with its momentum vector [27].

We build a multivariate BDT classifier to distinguish true signal candidates from continuum events, the main source of background. These continuum events feature a boosted jet-like topology whereas $B\overline{B}$ events result in a more isotropic distribution of final state particles. The different topologies are exploited in the BDT. The variables used for training the BDT are common between Belle and Belle II, but each BDT is trained independently. The signal MC samples are used as a proxy for signal while the continuum MC samples are used as a proxy for background. We use a total of eleven variables in the BDT: the polar angle of the signal B candidate in the c.m. frame, the angle between the B_{sig} thrust axis and the thrust axis of the rest of the event, and a total of nine modified Fox-Wolfram moments [28, 29]. We determine the optimal BDT output threshold by maximizing the signal significance, $N_S/\sqrt{N_S + N_B}$, where N_S and N_B denote the expected number of signal and background candidates, respectively, in a specific signal-enhanced window of $\Delta E \in [-0.2, 0.1]$ GeV and $M_{\mathrm{bc}} \in [5.27, 5.29]$ GeV/c^2. The BDT efficiency is about $65-70\%$ for signal and between $5-8\%$ for the continuum background.

There are multiple B_{sig} candidates in 15% of events. As the final step of the candidate selection procedure, we select a single B_{sig} candidate in each event. For Belle, we keep only the candidate with the best corrected χ^2 of the vertex fit using a variable, ξ, discussed in Ref. [30]. The ξ parameter is built specifically for time-dependent CP measurements in Belle, because using the χ^2 of the vertex fit directly would introduce a bias in the Δt distribution, since these are correlated. Unfortunately, the differences between the Belle and Belle II vertexing process makes ξ unusable for Belle II, as it has been found to introduce a bias. Thus, for Belle II, we randomly choose one candidate from the event. For events with multiple candidates these procedures select the correct candidate 45% (65%) of the time in Belle II (Belle). We check using simulated samples that none of the selection criteria biases the measurement of the time-dependent CP asymmetries.

Using the simulated MC samples we can estimate the ratios of our final selection efficiencies for the different modes present in the $B^0 \to K^0_{\mathrm{S}}\pi^+\pi^-\gamma$ decays:

$$R_{K^*} = \frac{\epsilon_{K^*}}{\epsilon_{K^0_{\mathrm{S}}\rho^0}}, \; R_{(K\pi)_0} = \frac{\epsilon_{(K\pi)_0}}{\epsilon_{K^0_{\mathrm{S}}\rho^0}}, \tag{4.1}$$

where ϵ_{K^*}, $\epsilon_{(K\pi)_0}$ and $\epsilon_{K^0_{\mathrm{S}}\rho^0}$ are the efficiencies of the decay modes quoted in Eq. 1.2, Eq. 1.3 and of the $f_{CP}\gamma$ decay, $B^0 \to K^0_{\mathrm{S}}\rho^0\gamma$, respectively. These efficiency ratios are expected to be insensitive to potential mismodeling of the detector to first order, since these processes result in a common set of final state particles. The estimated ratios are $R_{K^*} = 1.04 \pm 0.04$ (0.48 ± 0.03) and $R_{(K\pi)_0} = 1.00 \pm 0.04$ (0.35 ± 0.03) for the full selection without (with) the prompt pion pair mass, $m_{\pi^+\pi^-}$, requirement. This information is needed to compute the proportion of the CP mode with respect to the non-CP modes and thus determine the value of the mixing-induced CP observable $S_{K^0_S\rho^0}$.

The same procedure is applied to reconstruct and select our control mode $B^+ \to K^+\pi^+\pi^-\gamma$, which is also the isospin partner mode of $B^0 \to K^0_S\pi^+\pi^-\gamma$. We use it to validate different steps of the fit strategy. The candidate selection for this mode is performed in exactly the same manner as for the decay mode of interest, with the exception of requiring a K^+ instead of a K^0_S. The K^+ candidate must satisfy the same charged track requirements used for prompt pions, but must have PID information consistent with the kaon hypothesis. Since the K^0_S is not used to reconstruct the B^0 decay vertex, we do not use the K^+ track information to reconstruct the B^+ decay vertex.

5 Time-dependent CP fit strategy

5.1 Time-dependence and flavor tagger

The Δt distribution is sensitive to the CP parameters, C, S, S^+ and S^-. In Belle, the Δt observable is computed as $\Delta t = \Delta z/\beta\gamma c$, where $\Delta z \equiv z_{\rm sig} - z_{\rm tag}$ is the difference between the z positions of the $B_{\rm sig}$ and $B_{\rm tag}$ decay vertices and β and γ are the relativistic Lorentz factors. For Belle II, instead of Δz, we make use of Δl, the distance of the $B_{\rm sig}$ and $B_{\rm tag}$ decay-vertex positions along the $\Upsilon(4S)$ boost direction and calculate $\Delta t = \Delta l/\beta\gamma c$. For Belle, $\beta\gamma \approx 0.425$, while for Belle II $\beta\gamma \approx 0.284$, because the beam energy asymmetry is smaller. The precise value of $\beta\gamma$ is periodically calibrated using data. In Belle II we apply a correction [31] for the small boost of the B mesons in the c.m. frame [32], to account for the transverse component of the B flight in the laboratory frame. For Belle, the correction is not applied and the residual effect is taken into account as part of the resolution function [30].

To ensure an accurate extraction of the time-dependent CP asymmetry parameters, the physics probability density function (p.d.f.) is convolved with the finite Δt detector resolution, described by a resolution function $R(\Delta t)$. We use different parameterizations of the Δt resolution function for Belle and Belle II.

The Δt resolution function for Belle [30] is the combination of four individual contributions, arising from the resolution on the $B_{\rm sig}$ decay vertex position ($z_{\rm sig}$), the resolution on the $B_{\rm tag}$ decay vertex position ($z_{\rm tag}$), the resolution effects induced by tertiary vertices, in particular due to tracks stemming from D meson decays biasing the $B_{\rm tag}$ decay vertex, and lastly a contribution to correct for the small boost of the B mesons in the c.m. frame. The resolution function is conditional on several per-candidate observables of the fitted signal and tag vertices: the number of tracks, the number of degrees of freedom, χ^2 values and uncertainties on the longitudinal position of the vertices.

For Belle II, we parameterize the Δt resolution function by combining several Gaussian-like distributions with a per-candidate dependence on the Δt uncertainty, $\sigma_{\Delta t}$. The description of the resolution function and its calibration is detailed in Ref. [26].

The measurement of the time-dependent CP asymmetries requires the flavor of the decaying signal B meson. Since the $B_{\rm tag}$ and $B_{\rm sig}$ are entangled, by measuring the flavor of the tag B when it decays we can infer the flavor of the signal B. This premise is valid independently of which B meson decays first, i.e. Δt can assume negative values.

The $B_{\rm tag}$ decay products are input into dedicated multi-variate analysis tools referred to as flavor-tagging (FT) algorithms. Different FT algorithms are used for the Belle and Belle II measurements. We use the algorithm described in Ref. [33] for Belle, which achieves around a 30% effective tagging efficiency. For Belle II, we use a graph neural network to estimate the flavor of the $B_{\rm tag}$ meson, GFlat [26]. The GFlat algorithm provides an effective tagging efficiency of about 37%.

The FT algorithm provides the flavor prediction q ($q = 1$ for $B_{\rm tag} = B^0$ and $q = -1$ for $B_{\rm tag} = \overline{B}^0$) and the tag quality, r, which ranges from zero for no discriminating power to one for unambiguous flavor assignment. The imperfect assignment of the flavor by the FT algorithm is described by three parameters: the wrong-tag probability, w; the wrong-tag probability difference between B^0 and $\overline{B}^0$, Δw; and the tagging efficiency asymmetry between B^0 and $\overline{B}^0$, $a_{\rm tag}$. The values of these parameters are obtained through data-driven calibration in seven bins of tag-quality $r \approx 1-2w$ [26, 33]. The r-calibration binning is defined as $[0, 0.1, 0.25, 0.5, 0.625, 0.75, 0.875, 1]$ for Belle and as $[0, 0.1, 0.25, 0.45, 0.6, 0.725, 0.875, 1]$ for Belle II. For Belle, the calibration on the first bin $r \in [0, 0.1]$ provides no inherent flavor discrimination (i.e. $w \equiv 0.5$) so this bin is not used for the measurement of the time-dependent CP asymmetries. In both Belle and Belle II, the output of the FT algorithm is used on a per-candidate basis when performing the fit. Additionally, for Belle II, we split our sample into a good quality range $r \in [0, 0.875]$ and an excellent quality range $r \in [0.875, 1]$ and perform the fit simultaneously in these two r regions. This provides improved statistical sensitivity by accounting for the different background levels. For Belle, $a_{\rm tag}$ is neglected in the calibration procedure, whereas it is included in Belle II. The values of this parameter in both experiments are consistent with zero within uncertainties.

The p.d.f. describing the Δt distribution is:

$$\begin{aligned} P(\Delta t, q, w, \Delta w, a_{\rm tag}) = \frac{e^{-|\Delta t|/\tau_{B^0}}}{4\tau_{B^0}} \{ 1 - q\Delta w + q a_{\rm tag}(1-2w) \\ + [q(1-2w) + a_{\rm tag}(1 - q\Delta w)][S \sin(\Delta m \Delta t) - C \cos(\Delta m \Delta t)] \} \otimes R(\Delta t), \end{aligned} \tag{5.1}$$

where τ_{B^0} is the lifetime of B^0 meson, and $\otimes$ denotes the convolution of the physics p.d.f. with the resolution function, $R(\Delta t)$.

5.2 Extraction of the CP parameters

We measure the time-dependent CP asymmetries by performing an unbinned maximum likelihood fit in $M_{\rm bc}$, ΔE and Δt. The beam-energy constrained mass and energy difference, described previously, are powerful observables to disentangle the signal component from the background components. The Δt distribution is sensitive to the time-dependent CP asymmetries as previously discussed. The fit is performed independently for Belle and Belle II.

In addition to the signal component, three background sources are present in the fit region. The main background contribution is the one arising from continuum events:

while these events are highly suppressed by the candidate selection, a significant number still remains. The second background contribution is from misreconstructed $B\overline{B}$ decays, including both B^0 and B^+ decays. These include several B decays that can partially mimic our final state, mainly radiative B decays to two hadrons (K^0_S, $\pi^\pm$) plus a particle from the $B_{\rm tag}$ side. The third background source is self cross-feed (SCF): true $B^0 \to K^0_S\pi^+\pi^-\gamma$ signal decays that are incorrectly reconstructed. The leading source of SCF is when a pion from the $B_{\rm tag}$ is reconstructed as one of the signal prompt pions.

We model each of the four components using the simulated MC samples, independently in each of the fit observables ($M_{\rm bc}, \Delta E, \Delta t$). Two exceptions are discussed later, affecting the Δt distribution of continuum candidates and the $M_{\rm bc}$ and ΔE distributions of the contribution from misreconstructed $B\overline{B}$ candidates. The same modeling is used in the fit for Belle and Belle II if not otherwise stated. The parameters for the modeling are fixed to those determined in fits to the simulated MC samples if not otherwise stated. The models for each observable and component are presented in the following.

For the signal component, the $M_{\rm bc}$ and ΔE distributions are expected to peak at $M_{\rm bc} = m_{B^0}$ and $\Delta E = 0$, where m_{B^0} is the mass of the B^0 meson. We describe both distributions with Crystal Ball functions [34, 35], which combine a Gaussian core with power-law distributions for the tails. The mean and width parameters of the Gaussian cores are allowed to float freely in the fit to the data. The Δt fit function for the signal component was presented in Eq. 5.1. The values of the CP observables S and C are free parameters. The values of the B^0 lifetime and mass difference are fixed to the world-average values, $\tau_{B^0} = 1.517 \pm 0.004$ ps and $\Delta m = 0.5063 \pm 0.0019$ ps^{-1} [36] and their uncertainties are propagated as systematic uncertainties.

For the SCF component, the $M_{\rm bc}$ distribution is modeled by the sum of a bifurcated Gaussian distribution and an ARGUS p.d.f. [37]. We use a second order Chebychev polynomial to describe the ΔE distribution. For Belle II, we use a Chebychev polynomial with an additional bifurcated Gaussian distribution for improved modeling. The Δt distribution for the SCF component is also modeled with Eq. 5.1, with $S_{\rm SCF} = \kappa_{\rm SCF} \cdot S$ and $C_{\rm SCF} = \kappa_{\rm SCF} \cdot C$, where $\kappa_{\rm SCF}$ is common for both observables and is obtained from a fit to the simulated samples. In the unbinned maximum likelihood fit, a Gaussian constraint of mean 0.8 and width 0.2 is applied to $\kappa_{\rm SCF}$: this accounts for the statistical fluctuations of $\kappa_{\rm SCF}$ in the simulated samples.

For the continuum component we model the $M_{\rm bc}$ distribution using an ARGUS p.d.f. The threshold parameter of the ARGUS function is common to all contributions to the $M_{\rm bc}$ distribution and is free to float in the fit to the data. We model the ΔE distribution with an exponential function. Different approaches are taken to model the Δt distribution in Belle and Belle II. The Belle modeling uses the combination of a Gaussian distribution and an exponential convolved with a Gaussian [30]. We observe mismodeling between the Δt distribution in our continuum MC samples and the Δt distribution of the data samples below the $\Upsilon(4S)$ energy, where only continuum events are present. We correct our Δt distribution in the MC samples using weights obtained in 40 Δt bins from -10 ps to 10 ps. These weights are given by the ratio, in each Δt bin, of the yields of the data below the $\Upsilon(4S)$ energy to the continuum MC. We obtain the weights from the isospin partner mode.

For Belle II, the Δt distribution is modeled by the sum of three Gaussian functions, describing the core, the tail, and the outliers of the resolution. The widths of the core and tail Gaussians are free to float in the fit to the data.

The last background contribution, the misreconstructed $B\overline{B}$ component, is modeled differently in all three distributions for Belle and Belle II. In Belle, we model the $M_{\rm bc}$ distribution as the sum of a Gaussian and an ARGUS p.d.f. while we model the ΔE distribution with a sum of a Gaussian and an exponential distribution. The Δt distribution is modeled similarly to the continuum component, with a Gaussian and an exponential convolved with a Gaussian. It is worth noting that we find a similar quality of description if we instead use Eq. 5.1, with both C and S fixed to zero; this alternative is used to evaluate the systematic uncertainty. For Belle II, we describe the $M_{\rm bc}$ and ΔE distributions together using a kernel density estimator, to take into account small correlations between the two variables. The Δt distribution is modeled with Eq. 5.1 with both CP observables, C and S, fixed to zero. Most of the $B\overline{B}$ background arises from charged B meson decays and other radiative decays, thus the values of the CP parameters are expected to be zero or very close to it. The validity of this assumption is considered when assigning systematic uncertainties.

We allow three yields to be completely free in data when performing the unbinned maximum likelihood fit. The continuum component and the misreconstructed $B\overline{B}$ component have their yields free to float. The sum of the signal and SCF yields is free to float. The relative proportion of the signal and SCF components is fixed to the value extracted from the simulated MC samples. This value is around 29% for Belle. For Belle II it is 38% for the first r-region and 27% for the second r-region.

Additionally, for Belle II, as previously described, a simultaneous fit is performed in two regions of flavor tagging quality, r. The yields in each r bin are free to float. Consequently, for Belle we have a total of 10 free parameters: S, C, three yields, and five modeling parameters. In Belle II, we have 15 free parameters, due to the additional two free parameters in the Δt distribution of the continuum component and the three additional yields, due to the additional r-region.

The results of unbinned maximum likelihood fits to $M_{\rm bc}$, ΔE and Δt in the signal channel are $C = -0.04 \pm 0.11$ and $S = -0.18 \pm 0.17$, for the Belle dataset, and $C = -0.29 \pm 0.13$ and $S = -0.36 \pm 0.16$, for the Belle II dataset, where the uncertainties are statistical only. The correlations between the CP parameters are +4.8% for Belle and +10.4% for Belle II. We obtain 475 ± 31 signal candidates for Belle and 350 ± 23 for Belle II. The projections of the fit result in $M_{\rm bc}$ and ΔE are shown in Fig. 1 for Belle and Belle II. The projections on Δt are shown in Fig. 2. The Δt projections for B^0- and $\overline{B}^0$-tagged events are also shown, together with the asymmetry, in a signal enhanced region. The signal over background ratio in this region is about 3.4 for Belle and 2.4 for Belle II.

The same fit strategy is used to extract the CP observables using the two halves of the $(m^2(K^0_{\rm S}\pi^+), m^2(K^0_{\rm S}\pi^-))$ plane, S^+ and S^-. Candidates in the two halves of the plane are fit simultaneously. All free-floating parameters are common in the simultaneous fit to the two halves with the exception of the yields. This unbinned maximum likelihood fit is independent of the previous one. It has a total of 14 free floating parameters for Belle, due

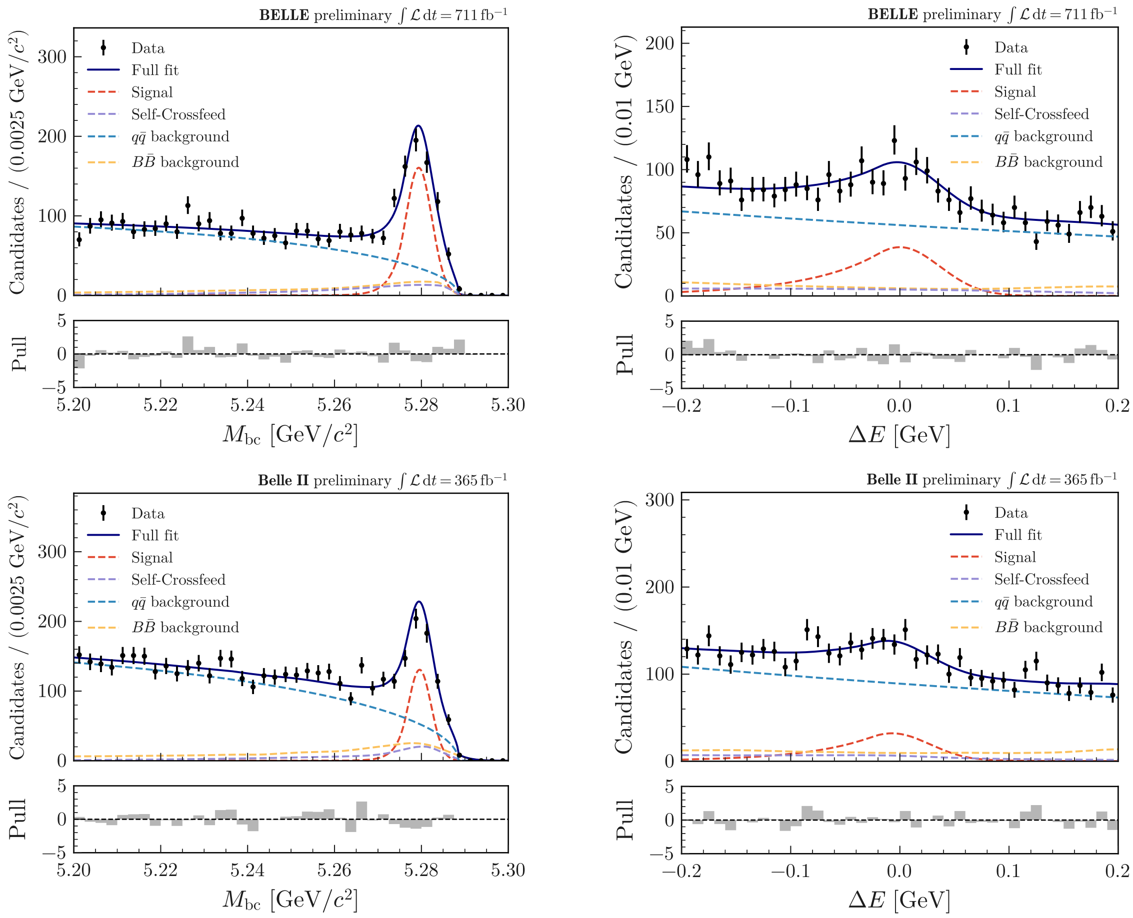

Figure 1. Unbinned maximum likelihood projections on $M_{\rm bc}$ (left) and ΔE (right) using the Belle (top) and Belle II (bottom) datasets.

to an additional *CP* observable: C, S^+ and S^- (instead of only C and S) and a total of six free floating yields instead of three. For Belle II the number of free-floating parameters rises to 22.

The results of the simultaneous unbinned maximum likelihood fit in the two half-planes are $S^+ = -0.33 \pm 0.34$ and $S^- = -0.36 \pm 0.38$ for Belle and $S^+ = -0.72 \pm 0.31$ and $S^- = 0.70 \pm 0.30$ for Belle II, with correlations of -5.9% and $+6.5\%$, respectively.

5.3 Validation and systematic uncertainties

We validate the fit strategy using the simulated MC samples for both the signal mode $B^0 \to K^0_{\rm S}\pi^+\pi^-\gamma$ and the control mode $B^+ \to K^+\pi^+\pi^-\gamma$. Then we validate on the data using the control mode and finally we perform the time-dependent *CP* asymmetry measurement.

The strategy for extracting the *CP* observables is first validated with MC samples. Using our nominal model, we create and fit a large number of data-like MC samples, with a luminosity equivalent to that used in the measurement, by resampling with replacement the combined MC samples of all components. The signal component in these data-like samples

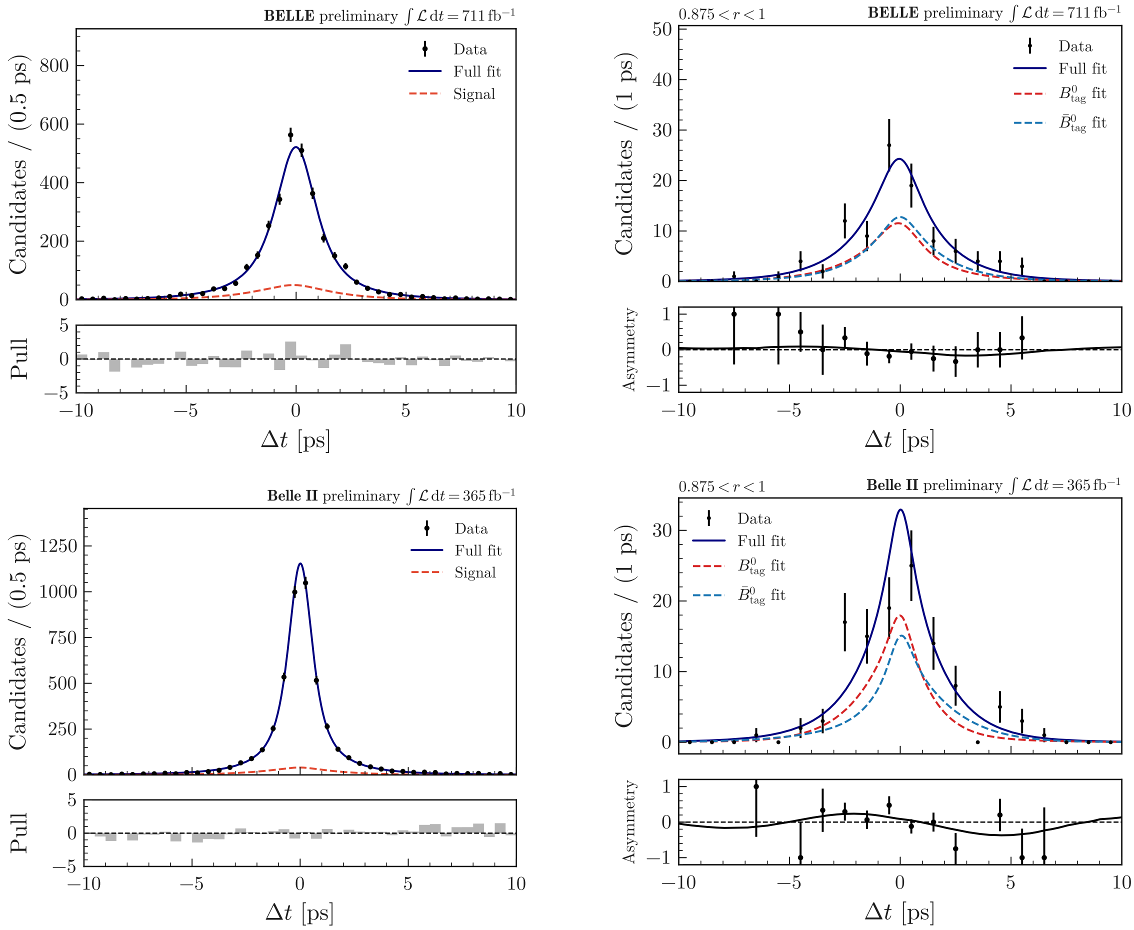

Figure 2. Unbinned maximum likelihood projection on Δt (left) and unbinned maximum likelihood projection on Δt split by tagged B^0 and $\overline{B}^0$ candidates in a signal enhanced window defined by: $M_{\rm bc} > 5.27$ GeV/c^2, $|\Delta E| < 0.1$ GeV and $r \in [0.875, 1]$ (right), using the Belle (top) and Belle II (bottom) dataset.

is generated with one of several different values of the mixing-induced *CP* observable, S. The differences between the fitted and expected values of the *CP* observables (and yields) from this validation process are taken as systematic uncertainties.

We perform the measurement of the time-dependent *CP* asymmetries in the control mode using the same procedure as for the signal mode, and the same values for the Δm and FT parameters. No time-dependent *CP* asymmetry is expected in B^+ decays; we find results for C and S compatible with zero within one standard deviation. Additionally, we fit for the B^+ lifetime and obtain, $\tau_{B^+} = 1.62 \pm 0.06$ (1.71 ± 0.06) ps for Belle II (Belle), which are compatible with the world average value within one standard deviation.

As a last validation step, we fit the B^0 lifetime in the data samples for $B^0 \to K^0_{\rm S}\pi^+\pi^-\gamma$ signal candidates, obtaining $\tau_{B^0} = 1.52$ $(1.47) \pm 0.11$ (0.10) ps for Belle II (Belle), compatible with the world-average value.

We consider several sources of systematic uncertainty that may affect the time-dependent

CP asymmetry measurement. These are computed independently for the Belle and Belle II datasets. We list the sources in Table 1 for Belle and Table 2 for Belle II. The majority of the uncertainties are evaluated by fitting the samples with alternative fit models and comparing the results to those from the nominal fit. The main systematic uncertainties arise from the vertex detector misalignment for Belle and the differences of the CP observables obtained as part of the validation process for Belle II.

We evaluate the systematic uncertainties arising from the parameterization of the fit distributions, the FT calibration, the resolution function model, and the usage of external parameters ($\tau_{B^0}, \Delta m$), in a similar manner. These are evaluated by fitting the data samples with alternative values of the corresponding fixed parameters. The alternative values are obtained by drawing values of each parameter from a normal distribution whose width is set by the parameter uncertainty or the covariance matrix obtained from MC simulated samples. The systematic uncertainty is computed as the standard deviation of the distribution of the fitted CP observables that are obtained from the alternative fits.

Additionally, we evaluate a systematic uncertainty due to the fixed ratio between the signal and the SCF by varying it by $\pm 20\%$ and refitting. This variation accounts for the statistical fluctuations of this ratio in the simulated samples. The shift in the CP observables is assigned as the systematic uncertainty.

We use the validation process to assign a systematic uncertainty due to possible biases on the extracted yields and CP observables. For the yields, we perform an alternative fit to the validation MC samples with the yields fixed to the generated values, and take the difference of the resulting CP observable values with respect to the nominal fit as the associated uncertainty. For the CP observables, we fit the validation MC samples using the nominal model and take the average deviation from the generated CP observables, for different values of S, as the systematic uncertainty. This uncertainty accounts for various contributing factors, including the limited size of the MC samples used in the validation as well as any discrepancies among the $M_{\rm bc}$, ΔE and Δt distributions in the MC samples and the models used to describe them. Although this systematic uncertainty is small compared to the statistical uncertainty, it remains the dominant contribution to the overall systematic uncertainty for Belle II.

A systematic uncertainty is computed for the tag-side-interference as described in Ref. [38]. This uncertainty is the only one that is correlated between Belle and Belle II.

A systematic uncertainty is computed for possible CP violation in the misreconstructed $B\overline{B}$ background component. The values of the assumed CP observables for the misreconstructed $B\overline{B}$ background are varied in the data samples: each of $C_{B\overline{B}}$ and $S_{B\overline{B}}$ is independently assigned a value of ± 0.1. The maximum difference of these four combinations relative to the nominal fit is assigned as the systematic uncertainty. The magnitude of this uncertainty is different between Belle and Belle II. The nominal Δt model for the misreconstructed $B\overline{B}$ background component for Belle, as previously presented, is not Eq. 5.1, whereas to compute this systematic we use Eq. 5.1 as the alternative model.

Lastly, we evaluate systematic uncertainties arising from a residual vertex detector misalignment: we reconstruct the B candidates with various misalignment scenarios using simulated MC samples, leading to slightly different fit results. These variations are performed separately for Belle and Belle II, given the intrinsic detector differences. In particular, for Belle, this irreducible source of systematic uncertainty is obtained for S and C, and the uncertainties for S^+ and S^- are computed from S as fully correlated. This uncertainty dominates the overall systematic uncertainty for Belle.

Table 1. Systematic uncertainties for the Belle measurement.

Source of uncertainty	C	S	S^+	S^-
Fixed shape parameters	0.003	0.002	0.004	0.004
Flavor Tagging parameters	0.003	0.002	0.006	0.006
Resolution function parameters	0.009	0.033	0.063	0.027
τ_{B^0} & Δm	0.001	0.001	0.002	0.002
Fixed SCF fraction	0.005	0.006	0.010	< 0.001
Yield bias	0.001	0.008	0.015	0.002
CP fit validation	0.018	0.019	0.035	0.075
Tag-side interference	0.028	< 0.001	< 0.001	< 0.001
CP violation in $B\overline{B}$ background	0.047	0.039	0.060	0.079
Residual misalignment	0.03	0.06	0.12	< 0.001
Total systematic uncertainty	0.066	0.081	0.153	0.112

Table 2. Systematic uncertainties for the Belle II measurement.

Source of uncertainty	C	S	S^+	S^-
Fixed shape parameters	0.003	0.005	0.005	0.004
Flavor Tagging parameters	0.018	0.007	0.014	0.012
Resolution function parameters	0.005	0.014	0.023	0.018
τ_{B^0} & Δm	< 0.001	0.001	0.001	0.003
Fixed SCF fraction	0.006	0.004	0.008	0.011
Yield bias	0.005	0.004	0.008	0.014
CP fit validation	0.027	0.054	0.117	0.033
Tag-side interference	0.028	< 0.001	< 0.001	< 0.001
CP violation in $B\overline{B}$ background	0.019	0.017	0.034	0.001
Residual misalignment	0.005	0.003	0.006	0.012
Total systematic uncertainty	0.048	0.059	0.126	0.045

6 Results and conclusions

The measured values of the CP parameters in the decay $B^0 \to K_S^0\pi^+\pi^-\gamma$ from the Belle data are:

$$\begin{aligned} C &= -0.04 \pm 0.11 \pm 0.07 \\ S &= -0.18 \pm 0.17 \pm 0.08 \\ S^+ &= -0.33 \pm 0.34 \pm 0.15 \\ S^- &= -0.36 \pm 0.38 \pm 0.11 \end{aligned} \tag{6.1}$$

Using the Belle II data we measure:

$$\begin{aligned} C &= -0.29 \pm 0.13 \pm 0.05 \\ S &= -0.36 \pm 0.16 \pm 0.06 \\ S^+ &= -0.72 \pm 0.31 \pm 0.13 \\ S^- &= 0.70 \pm 0.30 \pm 0.05 \end{aligned} \tag{6.2}$$

where the second term corresponds to the statistical uncertainty and the third term corresponds to the systematic uncertainty.

The measurements of S, C and S^+ are in agreement for the two experiments, and compatible with the SM prediction within 1σ for Belle, and 2.3σ for Belle II. The values obtained for S^- are in slight tension (2.2σ apart), but are independently compatible with the SM prediction of zero.

We combine the results following the method presented in Ref. [39], taking into account the correlations between the measured CP parameters. We consider all sources of systematic uncertainty as uncorrelated, except the tag-side-interference, which is fully correlated. The combined results are:

$$\begin{aligned} C &= -0.17 \pm 0.09 \pm 0.04 \\ S &= -0.29 \pm 0.11 \pm 0.05 \\ S^+ &= -0.57 \pm 0.23 \pm 0.10 \\ S^- &= 0.31 \pm 0.24 \pm 0.05 \end{aligned} \tag{6.3}$$

The correlation between C and S is -3%, while the correlation between S^+ and S^- is $+2\%$.

Our combined measurement of S and C improves by at least a factor of two the corresponding uncertainties on the CP observables measured previously by the Belle and BaBar collaborations. This result supersedes the time-dependent CP asymmetry, namely $\mathcal{S}_{\text{eff}}$, presented in Ref. [5]. We also measure, for the first time, the CP parameters S^+ and S^-, which are needed to apply additional constraints to new physics models with enhanced right-handed currents that may affect the $B^0 \to K_S^0\pi^+\pi^-\gamma$ transition.

This work, based on data collected using the Belle II detector, which was built and commissioned prior to March 2019, and data collected using the Belle detector, which was operated until June 2010, was supported by Higher Education and Science Committee of the Republic of Armenia Grant No. 23LCG-1C011; Australian Research Council and Research Grants No. DP200101792, No. DP210101900, No. DP210102831, No. DE220100462, No. LE210100098, and No. LE230100085; Austrian Federal Ministry of Education, Science and Research, Austrian Science Fund (FWF) Grants DOI: 10.55776/P34529, DOI: 10.55776/J4731, DOI: 10.55776/J4625, DOI: 10.55776/M3153, and DOI: 10.55776/PAT1836324, and Horizon 2020 ERC Starting Grant No. 947006 "InterLeptons"; Natural Sciences and Engineering Research Council of Canada, Digital Research Alliance of Canada, and Canada Foundation for Innovation; National Key R&D Program of China under Contract No. 2024YFA1610503, and No. 2024YFA1610504 National Natural Science Foundation of China and Research Grants No. 11575017, No. 11761141009, No. 11705209, No. 11975076, No. 12135005, No. 12150004, No. 12161141008, No. 12405099, No. 12475093, and No. 12175041, and Shandong Provincial Natural Science Foundation Project ZR2022JQ02; the Czech Science Foundation Grant No. 22-18469S, Regional funds of EU/MEYS: OPJAK FORTE CZ.02.01.01/00/22_008/0004632 and Charles University Grant Agency project No. 246122; European Research Council, Seventh Framework PIEF-GA-2013-622527, Horizon 2020 ERC-Advanced Grants No. 267104 and No. 884719, Horizon 2020 ERC-Consolidator Grant No. 819127, Horizon 2020 Marie Sklodowska-Curie Grant Agreement No. 700525 "NIOBE" and No. 101026516, and Horizon 2020 Marie Sklodowska-Curie RISE project JENNIFER2 Grant Agreement No. 822070 (European grants); L'Institut National de Physique Nucléaire et de Physique des Particules (IN2P3) du CNRS and L'Agence Nationale de la Recherche (ANR) under Grant No. ANR-23-CE31-0018 (France); BMFTR, DFG, HGF, MPG, and AvH Foundation (Germany); Department of Atomic Energy under Project Identification No. RTI 4002, Department of Science and Technology, and UPES SEED funding programs No. UPES/R&D-SEED-INFRA/17052023/01 and No. UPES/R&D-SOE/20062022/06 (India); Israel Science Foundation Grant No. 2476/17, U.S.-Israel Binational Science Foundation Grant No. 2016113, and Israel Ministry of Science Grant No. 3-16543; Istituto Nazionale di Fisica Nucleare and the Research Grants BELLE2, and the ICSC – Centro Nazionale di Ricerca in High Performance Computing, Big Data and Quantum Computing, funded by European Union – NextGenerationEU; Japan Society for the Promotion of Science, Grant-in-Aid for Scientific Research Grants No. 16H03968, No. 16H03993, No. 16H06492, No. 16K05323, No. 17H01133, No. 17H05405, No. 18K03621, No. 18H03710, No. 18H05226, No. 19H00682, No. 20H05850, No. 20H05858, No. 22H00144, No. 22K14056, No. 22K21347, No. 23H05433, No. 26220706, and No. 26400255, and the Ministry of Education, Culture, Sports, Science, and Technology (MEXT) of Japan; National Research Foundation (NRF) of Korea Grants No. 2021R1-F1A-1064008, No. 2022R1-A2C-1003993, No. 2022R1-A2C-1092335, No. RS-2016-NR017151, No. RS-2018-NR031074, No. RS-2021-NR060129, No. RS-2023-00208693, No. RS-2024-00354342 and No. RS-2025-02219521, Radiation Science Research Institute, Foreign Large-Size Research Facility Application Supporting project, the Global Science Experimental Data Hub Center, the Korea Institute of Science and Technology Information (K25L2M2C3) and KREONET/GLORIAD; Universiti Malaya RU grant, Akademi Sains Malaysia, and Ministry of Education Malaysia; Frontiers of Science Program Contracts No. FOINS-296, No. CB-221329, No. CB-236394, No. CB-254409, and

No. CB-180023, and SEP-CINVESTAV Research Grant No. 237 (Mexico); the Polish Ministry of Science and Higher Education and the National Science Center; the Ministry of Science and Higher Education of the Russian Federation and the HSE University Basic Research Program, Moscow; University of Tabuk Research Grants No. S-0256-1438 and No. S-0280-1439 (Saudi Arabia), and Researchers Supporting Project number (RSPD2025R873), King Saud University, Riyadh, Saudi Arabia; Slovenian Research Agency and Research Grants No. J1-50010 and No. P1-0135; Ikerbasque, Basque Foundation for Science, State Agency for Research of the Spanish Ministry of Science and Innovation through Grant No. PID2022-136510NB-C33, Spain, Agencia Estatal de Investigacion, Spain Grant No. RYC2020-029875-I and Generalitat Valenciana, Spain Grant No. CIDEGENT/2018/020; the Swiss National Science Foundation; The Knut and Alice Wallenberg Foundation (Sweden), Contracts No. 2021.0174, No. 2021.0299, and No. 2023.0315; National Science and Technology Council, and Ministry of Education (Taiwan); Thailand Center of Excellence in Physics; TUBITAK ULAKBIM (Turkey); National Research Foundation of Ukraine, Project No. 2020.02/0257, and Ministry of Education and Science of Ukraine; the U.S. National Science Foundation and Research Grants No. PHY-1913789 and No. PHY-2111604, and the U.S. Department of Energy and Research Awards No. DE-AC06-76RLO1830, No. DE-SC0007983, No. DE-SC0009824, No. DE-SC0009973, No. DE-SC0010007, No. DE-SC0010073, No. DE-SC0010118, No. DE-SC0010504, No. DE-SC0011784, No. DE-SC0012704, No. DE-SC0019230, No. DE-SC0021274, No. DE-SC0021616, No. DE-SC0022350, No. DE-SC0023470; and the Vietnam Academy of Science and Technology (VAST) under Grants No. NVCC.05.02/25-25 and No. DL0000.05/26-27.

These acknowledgements are not to be interpreted as an endorsement of any statement made by any of our institutes, funding agencies, governments, or their representatives.

We thank the SuperKEKB team for delivering high-luminosity collisions; the KEK cryogenics group for the efficient operation of the detector solenoid magnet and IBBelle on site; the KEK Computer Research Center for on-site computing support; the NII for SINET6 network support; and the raw-data centers hosted by BNL, DESY, GridKa, IN2P3, INFN, PNNL/EMSL, and the University of Victoria.

References

[1] D. Atwood, M. Gronau and A. Soni, *Mixing induced CP asymmetries in radiative B decays in and beyond the standard model*, *Phys. Rev. Lett.* **79** (1997) 185 [hep-ph/9704272].

[2] E. Kou, C.-D. Lü and F.-S. Yu, *Photon Polarization in the $b \to s\gamma$ processes in the Left-Right Symmetric Model*, *JHEP* **12** (2013) 102 [1305.3173].

[3] N. Haba, H. Ishida, T. Nakaya, Y. Shimizu and R. Takahashi, *Search for new physics via photon polarization of $b \to s\gamma$*, *JHEP* **03** (2015) 160 [1501.00668].

[4] BaBar collaboration, *Time-dependent analysis of $B^0 \to K^0_S\pi^-\pi^+\gamma$ decays and studies of the $K^+\pi^-\pi^+$ system in $B^+ \to K^+\pi^-\pi^+\gamma$ decays*, *Phys. Rev. D* **93** (2016) 052013 [1512.03579].

[5] Belle collaboration, *Time-dependent CP Asymmetries in $B^0 \to K^0_S\rho^0\gamma$ Decays*, *Phys. Rev. Lett.* **101** (2008) 251601 [0806.1980].

[6] S. Akar, E. Ben-Haim, J. Hebinger, E. Kou and F.-S. Yu, *The time-dependent CP asymmetry in* $B^0 \to K_{\rm res}\gamma \to \pi^+\pi^- K_S^0\gamma$ *decays*, *JHEP* **09** (2019) 034 [1802.09433].

[7] A. Abashian et al., *The BELLE detector*, *Nucl. Instrum. Meth. A* **479** (2002) 117.

[8] Belle collaboration, *Physics Achievements from the Belle Experiment*, *PTEP* **2012** (2012) 04D001 [1212.5342].

[9] T. Abe et al., *Achievements of KEKB*, *PTEP* **2013** (2013) 03A001.

[10] Belle II collaboration, *Belle II technical design report*, 1011.0352.

[11] K. Akai, K. Furukawa and H. Koiso, *SuperKEKB collider*, *Nucl. Instrum. Meth. A* **907** (2018) 188 [1809.01958].

[12] Belle II SVD collaboration, *The design, construction, operation and performance of the Belle II silicon vertex detector*, *JINST* **17** (2022) P11042 [2201.09824].

[13] D. Kotchetkov et al., *Front-end electronic readout system for the Belle II imaging Time-Of-Propagation detector*, *Nucl. Instrum. Meth. A* **941** (2019) 162342 [1804.10782].

[14] D.J. Lange, *The EvtGen particle decay simulation package*, *Nucl. Instrum. Meth. A* **462** (2001) 152.

[15] T. Sjöstrand, S. Ask, J.R. Christiansen, R. Corke, N. Desai, P. Ilten et al., *An Introduction to PYTHIA 8.2*, *Comput. Phys. Commun.* **191** (2015) 159 [1410.3012].

[16] S. Jadach, B.F.L. Ward and Z. Wąs, *The precision Monte Carlo event generator KK for two-fermion final states in* e^+e^- *collisions*, *Comput. Phys. Commun.* **130** (2000) 260 [hep-ph/9912214].

[17] GEANT4 collaboration, *GEANT4: A simulation toolkit*, *Nucl. Instrum. Meth. A* **506** (2003) 250.

[18] P.M. Lewis et al., *First Measurements of Beam Backgrounds at SuperKEKB*, *Nucl. Instrum. Meth. A* **914** (2019) 69 [1802.01366].

[19] Belle II collaboration, "Belle II Analysis Software Framework (basf2)." https://doi.org/10.5281/zenodo.5574115.

[20] Belle II Framework Software Group collaboration, *The Belle II Core Software*, *Comput. Softw. Big Sci.* **3** (2019) 1 [1809.04299].

[21] Belle collaboration, *An inclusive measurement of the photon energy spectrum in* $b \to s\gamma$ *decays*, *Phys. Rev. Lett.* **93** (2004) 061803 [hep-ex/0403004].

[22] Belle II collaboration, *Measurement of branching fractions, CP asymmetry, and isospin asymmetry for* $B \to \rho\gamma$ *decays using Belle and Belle II data*, *Phys. Rev. D* **111** (2025) L071103 [2407.08984].

[23] M. Feindt and U. Kerzel, *The NeuroBayes neural network package*, *Nucl. Instrum. Meth. A* **559** (2006) 190.

[24] Belle collaboration, *Measurement of time-dependent CP asymmetries in* $B^0 \to K_S^0\eta\gamma$ *decays*, *Phys. Rev. D* **97** (2018) 092003 [1803.07774].

[25] Belle II collaboration, *Measurement of CP asymmetries in* $B^0 \to K_S^0\pi^0\gamma$ *decays at Belle II*, *Phys. Rev. Lett.* **134** (2025) 011802 [2407.09139].

[26] Belle II collaboration, *New graph-neural-network flavor tagger for Belle II and measurement of* $\sin 2\phi_1$ *in* $B^0 \to J/\psi K_S^0$ *decays*, *Phys. Rev. D* **110** (2024) 012001 [2402.17260].

[27] S. Dey and A. Soffer, *Beam-Constrained Vertexing for B Physics at the Belle II Experiment*, *Springer Proc. Phys.* **248** (2020) 411.

[28] G.C. Fox and S. Wolfram, *Observables for the analysis of event shapes in* e^+e^- *annihilation and other processes*, *Phys. Rev. Lett.* **41** (1978) 1581.

[29] Belle collaboration, *Evidence for* $B^0 \to \pi^0\pi^0$, *Phys. Rev. Lett.* **91** (2003) 261801 [hep-ex/0308040].

[30] H. Tajima et al., *Proper time resolution function for measurement of time evolution of B mesons at the KEK B factory*, *Nucl. Instrum. Meth. A* **533** (2004) 370 [hep-ex/0301026].

[31] Belle II collaboration, *Observation of time-dependent CP violation and measurement of the branching fraction of* $B^0 \to J/\psi\pi^0$ *decays*, *Phys. Rev. D* **111** (2025) 012011 [2410.08622].

[32] Ed. A. J. Bevan, B. Golob, Th. Mannel, S. Prell, and B. D. Yabsley, *The physics of the B factories*, *Eur. Phys. J.* **C74** (2014) 3026 [1406.6311].

[33] Belle collaboration, *Neutral B flavor tagging for the measurement of mixing induced CP violation at Belle*, *Nucl. Instrum. Meth. A* **533** (2004) 516 [hep-ex/0403022].

[34] J. Gaiser, *Charmonium spectroscopy from radiative decays of the* J/ψ *and* ψ', Ph.D. thesis, Stanford University, 1982.

[35] T. Skwarnicki, *A study of the radiative CASCADE transitions between the Upsilon-Prime and Upsilon resonances*, Ph.D. thesis, Cracow, INP, 1986.

[36] Particle Data Group collaboration, *Review of particle physics*, *Phys. Rev. D* **110** (2024) 030001.

[37] ARGUS collaboration, *Search for Hadronic* $b \to u$ *Decays*, *Phys. Lett. B* **241** (1990) 278.

[38] O. Long, M. Baak, R.N. Cahn and D.P. Kirkby, *Impact of tag side interference on time dependent CP asymmetry measurements using coherent* $B^0\,\overline{B}^0$ *pairs*, *Phys. Rev. D* **68** (2003) 034010 [hep-ex/0303030].

[39] Heavy Flavor Averaging Group (HFLAV) collaboration, *Averages of b-hadron, c-hadron, and* τ*-lepton properties as of 2023*, 2411.18639.